Desalination 273 (2011) 276–284

Contents lists available at ScienceDirect

Desalination

journal homepage: www.elsevier.com/locate/desal

Characterization of the structural properties and Pb(II) adsorption behavior of iron oxide coated sepiolite

E. Eren *, H. Gumus

Bilecik University, Faculty of Science and Arts, Department of Chemistry, 11210, Bilecik, Turkey

ARTICLE INFO

Article history:
Received 13 September 2010
Received in revised form 27 December 2010
Accepted 4 January 2011

Keywords:
Sepiolite
Adsorption
Thermodynamic
Clay
Lead ions

ABSTRACT

This paper presents the adsorption of Pb(II) from aqueous solution by raw sepiolite (RS) and iron oxide-coated sepiolite (ICS) samples. Adsorption of Pb(II) by RS and ICS sample was investigated as a function of the initial Pb(II) concentration, solution pH, ionic strength, temperature and inorganic ligand (Cl^-). Changes in the surfaces and structure of sepiolite samples were characterized by means of IR and thermal analysis (TG-DTA). The perturbation observed on the zeolitic and bound water vibrations of ICS indicates that some of iron oxide particles enter the interior channels and replace zeolitic water molecules. The exothermal peak at 834 °C for RS and at 774 °C for ICS in the thermal analysis curves is assigned to the phase transformation of sepiolite to enstatite ($MgSiO_3$). The Langmuir monolayer adsorption capacities of RS and ICS in 0.1 M $NaNO_3$ solution at 298 K were estimated as 5.36 and 75.79 mg/g, respectively. Thermodynamic parameters such as change in free energy (ΔG), enthalpy (ΔH) and entropy (ΔS) were evaluated for RS and ICS to be −15.46 kJ/mol (at 298 K), 47.78 kJ/mol and 212 J/mol K, and −16.03 kJ/mol (at 298 K), 47.48 kJ/mol and 213 J/mol K, respectively.

1. Introduction

Metal oxides is typically thought to be the most important adsorbent for removal of heavy metals in aqueous solution due to their relatively high surface area, microporous structure, and OH functional groups adsorbing the metal cations [1–3]. However, solid separation and sludge management after the metal adsorption on oxides is difficult, because the oxides are usually in colloidal forms. One possible solution to this problem is to prepare a coated adsorbent. Iron oxide coated materials for heavy metal removal have been proved successful for the enhancement of treatment capacity and efficiency when compared with uncoated adsorbent, such as silica sand [4,5], activated carbon [6,7] and clay [8].

Sepiolite ($Si_{12}O_{30}Mg_8(OH)_4(H_2O)_4 \cdot 8H_2O$) is a natural fibrous clay mineral with hydrated magnesium silicate structure [9]. The structure of sepiolite is nearly similar to those of other 2:1 trioctahedral silicates, but it has discontinuity of the silica sheets, which gives rise to structural tunnels and blocks. These tunnels contain H_2O molecules and exchangeable cations such as Na^+, K^+, and Ca^{2+}. In the inner blocks, all corners of the silica tetrahedral are connected to adjacent blocks, but in the outer blocks, some of the corners are Si atoms bound to hydroxyls (Si—OH). These Si—OH groups are the main active centers for adsorption [10–12]. This different structure assigns an industrial importance in adsorptive, catalytic and rheological applications for sepiolite [13–29]. Sepiolite has different uses due to its unique structure, such as catalyst carrier [13–15], filler in polymer composites [16–18], membrane for ultrafiltration [19,20], adsorbent for organic molecules and heavy-metals [21–24], molecular sieve [25,26], and inorganic template [27–29].

Sepiolite, which has a high surface area, should provide an efficient surface for the iron oxides. At the same time, the iron oxides can improve the heavy metal adsorption capacity of sepiolite. To our knowledge, however, so far there has been no report in the literature about the interaction between Pb(II) and iron oxide-coated sepiolite (ICS). For these reasons, the aim of this paper is to examine the effectiveness of iron oxide-coated sepiolite (ICS) in removing Pb(II) from aqueous solution and to determine the adsorption characteristics of Pb(II) onto the ICS sample. The influence of pH, ionic strength, ligand (Cl^-) and temperature on the adsorption of Pb(II) by the raw sepiolite (RS) and ICS samples was investigated to better understand the Pb(II) adsorption process. The materials were characterized by infrared spectroscopy (IR) and thermal analysis (TG-DTA) techniques.

2. Experimental

2.1. Materials

All reagents, such as NaCl, $NaNO_3$, HNO_3, NaOH, and $Fe(NO_3)_3 \cdot 9H_2O$ were all of analytical grade and all solutions were prepared with double distilled water. A solution of 1.0 mM Pb(II) was prepared from $Pb(NO_3)_2$ by dissolution in deionized water. The stock solution was diluted to prepare a working solution.

* Corresponding author. Tel.: +90 228 2160101; fax: +90 228 2160287.
E-mail address: erdal.eren@bilecik.edu.tr (E. Eren).

0011-9164/$ – see front matter © 2011 Elsevier B.V. All rights reserved.
doi:10.1016/j.desal.2011.01.004

The preparations of the iron oxide coated clay sample have already been discussed in a previous work [30]. The system was prepared by mixing 20.0 g of RS, 100 ml of freshly prepared 1.0 M $Fe(NO_3)_3 \cdot 9H_2O$ solution, and 180 ml of 2.0 M NaOH solution in a 2-L polyethylene flask. The addition of NaOH solution was rapid and with stirring. The suspension was diluted to 2 L with twice distilled water and was held in a Pyrex glass beaker flask at 80 °C for 48 h.

Infrared (IR) spectra of the sepiolite samples were recorded in the region 4000 to 450 cm^{-1} on a Spectrum-100 FTIR spectrometer. The thermal gravimetric (TG) and differential thermal analyses (DTA) curves were obtained using a PRIS Diamond TG/DTG apparatus in a static air atmosphere (heating rate: 10 °C min^{-1}, platinum crucibles, mass ~10 mg and temperature range: 30–1000 °C).

2.2. Adsorption dependence on Pb(II) concentration

The adsorption of Pb(II) by sepiolite samples was performed by a batch equilibrium technique at room temperature. Briefly, 0.050 g of sepiolite sample and 20 ml of $Pb(NO_3)_2$ solution were added in 50 ml polypropylene centrifuge tubes. In the present work, adsorption could not be carried out beyond pH 6.0 due to precipitation of $Pb(OH)_2$ and therefore, the experiments were done in the pH range 3.0–5.5. The results reveal that adsorption increases with the increase in pH from 3.0 to 5.5 and the maximum adsorption is at pH 5.5, but we chose pH 5.0 to avoid hydrolysis of Pb(II). Ionic strength controlled at 0.1 M KNO_3 and the pH of the system was maintained at 5.0. The initial Pb(II) concentrations varied from 0.01 to 1.0 mM. A 24-h contacting period was found to be sufficient to achieve equilibrium. All the measurements were made in duplicate. For each sample, an experiment without adsorbent was performed to test possible adsorption and/or precipitation of metals onto the container walls. Preliminary experiments showed that metal losses due to the adsorption onto the container walls and to the filter paper were negligible. The adsorption isotherm experiments were repeated in triplicate and the average values were reported. Adsorbed Pb(II) was calculated from the difference between the Pb(II) initially added to the system and that remaining in the solution after equilibration by a Unicam 929 model flame atomic absorption spectrophotometer. The dilutions induced by the pH controls were considered while computing the amount of Pb(II) adsorbed.

2.3. Effect of ionic strength, pH, inorganic ligand and temperature

Adsorption experiments were carried out in polyethylene test tubes at 23 ± 2 °C by using the batch technique. The reaction mixture consisted of a total of 50 mL containing 1 g/L adsorbent and the desired concentration of Pb(II) ions. A solution of 1.0 mM Pb(II) was prepared from $Pb(NO_3)_2$ by dissolving in deionized water. The stock was diluted to prepare a working solution of 0.5 mM Pb(II). The ionic strength dependence of lead's removal from solution by sepiolite samples is used to distinguish between non-specific and specific adsorption. Also, this might indicate that the influence of the ionic strength on the activity coefficients of lead ions, which limit their transfer to the adsorbent surfaces. The ionic strengths of 0.01, 0.05 and 0.1 M $NaNO_3$ were used to test their effects on Pb(II) adsorbed by RS and ICS at various initial Pb(II) concentrations. Solution pH was adjusted with 0.1 M HNO_3 or 0.1 M NaOH, such that the equilibrium solutions had pH values ranging from 3.0 to 5.5. Preliminary kinetic studies indicated that Pb(II) adsorption was characterized by a rapid initial adsorption (within 1 h) followed by a much slower, continuous uptake. A 24-h contacting period was found to be sufficient to achieve equilibrium. The separation of the liquid from the solid phase was achieved by centrifugation at 4500 rpm for 20 min. The presence of co-ions in solution can affect the adsorption of metal ions onto a charged surface. In this study, the effect of co-ions in solution on adsorption capacity was also investigated. NaCl was chosen and added to the Pb(II) solutions at a concentration of 0.01 M. Pb(II) adsorption in the presence of Cl^- was performed by equilibrating 0.05 g of sepiolite sample in 20 mL of 0.25 M $NaNO_3$ background electrolyte, 10 mL of Pb(II) working solution, and 20 mL of a NaCl working solution (achieving 0.01 M Cl^-) in 50-mL polyethylene test tubes. These experiments were performed in duplicate. The temperature was varied from 298 K to 318 K at a constant pH of 5.0. For these experiments, 1 g/L of sepiolite samples with 124.7 mg/L Pb(II) solutions was employed.

2.4. Desorption studies

In this experiment, desorption of Pb(II) from Pb-loaded sepiolite samples was performed using HNO_3 solution at different concentrations. Pb-loaded sepiolite was exposed to a 50 mL solution of different HNO_3 concentrations (0.001, 0.005, 0.01 and 0.1 M HNO_3) in a batch experimental study at 298 K for 2 h. The supernatant was decanted for Pb(II) concentration measurement. Also, desorption experiments were performed using 0.1 M HNO_3 in a batch experimental study. The Pb(II)-loaded RS and ICS were washed with deionized water, respectively, to remove any unadsorbed Pb(II). The RS and ICS were then re-suspended in 50 ml of 0.1 M HNO_3 following the same equilibrium condition for the adsorption process. The solution mixture was filtered and the adsorbent washed several times with distilled water in order to remove excess acid. It was then treated with 50 ml of Pb(II) solution and the above procedure was repeated for three cycles using the same adsorbents. All experiments were carried out in triplicate with the mean of the results reported.

2.5. Data processing

The adsorption percentage of Pb(II) was calculated by the difference of the initial and final concentrations using the following equation:

$$R = \frac{(C_0 - C_e)}{C_0} \times 100 \quad (1)$$

where C_0 is the initial concentration of Pb(II) solution (mg/L), C_e is the equilibrium concentration of the Pb(II) solution (mg/L), and R is the adsorbed percentage of Pb(II).

The equilibrium data have been analyzed using the Langmuir and Freundlich isotherms and the characteristic parameters for each isotherm have been determined [31,32]. The data conform to the linear form of the Langmuir model [31] (Eq. (2)) expressed below:

$$C_e / q_e = C_e/q_m + 1/K_L q_m \quad (2)$$

where C_e is the equilibrium concentration of Pb(II) (mg/L) and q_e is the amount of the Pb^{2+} adsorbed (mg) per unit of sepiolite (g). q_m and K_L are the Langmuir constants related to the adsorption capacity (mg/g) and the equilibrium constant (L/g), respectively.

The adsorption equilibrium data was also applied to the Freundlich model [32] (Eq. (3)) given below:

$$\log q_e = \log K_F + (1/n)\log C_e \quad (3)$$

where K_F and *n* are the Freundlich constants related to adsorption capacity and adsorption intensity, respectively. The Freundlich parameters (K_F and n) indicate whether the nature of adsorption is either favorable or unfavorable.

The thermodynamic parameters of the adsorption process can be determined from the experimental data as described before [33]. The amount of Pb(II) ions adsorbed at equilibrium at different

temperatures is 298, 308 and 318 K, have been examined to obtain the thermodynamic parameters for the adsorption system.

$$\ln K_d = \Delta S / R - \Delta H / RT \quad (4)$$

$$\Delta G = \Delta H - T\Delta S \quad (5)$$

$$K_d = q_e / C_e \quad (6)$$

where K_d is the distribution coefficient for the adsorption, ΔS, ΔH and ΔG are the changes of entropy, enthalpy and Gibbs energy, T (K) is the temperature, and R (J mol^{-1} K^{-1}) is the gas constant. The values of ΔH and ΔS were determined from the slopes and intercepts of plots of ln K_d vs. 1/T.

The desorption of Pb(II) from the solid phase was calculated as follows:

$$Pb(II)desorbed(\%) = \frac{C_d}{C_a} \times 100 \quad (7)$$

where C_d and Ca are the amount of Pb(II) released into the aqueous solution and the amount of Pb(II) adsorbed onto sepiolites (mg/L), respectively.

3. Results and discussion

3.1. Material characterization

When the IR spectra of the samples are compared, some important differences in the band positions and intensities of RS and ICS samples are observed (Fig. 1a and b). These changes indicate the interaction between the iron oxide and sepiolite particles (Table 1).

The spectrum of the RS showed the band at 3686 cm^{-1} corresponding to Mg–OH vibration inside the sepiolite block and the band at 3571 cm^{-1} assigned to the vibrations of water coordinated to the Mg^{2+} ions located at the edges of the structural blocks (Fig. 1a). As shown in Fig. 1b, the bands at 3686 and 3571 cm^{-1} disappeared, after iron oxide coating process. This result showed that Mg^{2+} cations were removed losing the water and hydroxyl group coordinated to them during the oxide coating process. This corresponds to the Mg^{2+} cations located at the edges of the octahedral layers. As shown in Fig. 1b, the decreasing intensity of the hydroxyl vibration of the zeolitic water (3437 cm^{-1}) indicates the replacement iron oxide particles with part of the zeolitic water. IR spectrum of the iron oxide coated sepiolite shows the change of the absorption band related to the H—O—H bending vibration of water molecules adsorbed on ICS. The position of this band shifts from 1656 cm^{-1} (with a shoulder at 1695 cm^{-1}) to 1643 cm^{-1}. This result indicates the decrease of the H_2O content with the replacement of iron oxide molecules. The bands at 1204 and 1015 cm^{-1} form as a result of the Si—O vibrations. The peak at 1204 cm^{-1} only appears in palygorskite and sepiolite but not in lamellar clay minerals [34] and is from Si—O—Si bond between the alternative ribbons.

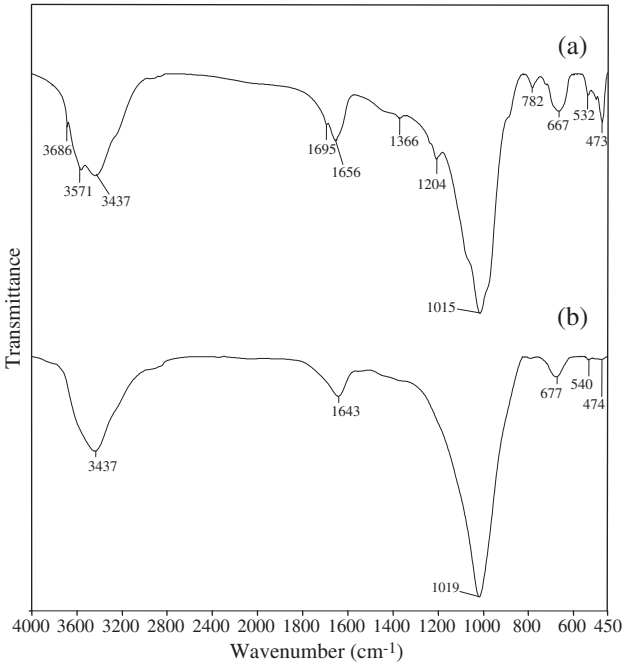

Fig. 1. IR spectra of the RS (a) and ICS (b) samples.

Table 1
Infrared absorption bands of sepiolite samples.

Suggested assignments [29,30]	RS	ICS	RS-Pb(II)	ICS-Pb(II)
MgOH (trioctahedral) stretch	3686 (vw)	–	3686 (vw)	–
OH-stretch from coordinated water	3571 (s)	–	3571 (sh)	
Zeolitic water	3437 (s,br)	3437 (vs, br)	3437 (s, w)	3437 (s,br)
Water OH bend	1695 (sh)	–	1698 (sh)	–
Water OH bend	1656 (m)	1643 (m, br)	1650 (m, br)	1633 (m, br)
SiO stretch	1204 (w)	–	1204 (w)	–
SiO stretch	1015(vs)	1019 (vs)	1016 (vs)	1019 (br)
OH deformation	782 (m)	–	776 (w)	–
OH translation	667 (m, br)	667 (m, br)	668 (m, br)	669 (m)
OSiO bends	532 (w)	540 (w, br)	537 (m)	–
OSiO bends	473 (m)	474 (vw, br)	473 (m)	–

w: weak, m: middle, s:strong, vs: very strong, vw: very weak, br: broad.

IR spectrum of the ICS sample showed that this peak disappeared after iron oxide coating process. This result reveals the formation of iron oxide/sepiolite covalent bonds, it also confirms that the new material maintains the basic structure of sepiolite. Noticeable changes were also detected for bands in the region between 900 and 400 cm^{-1}, after iron oxide coating process. These changes do not result only in a shift of band positions but mainly in their intensities, which are decreased. The Si—O stretching bands of ICS sample also showed a gradual decrease in the intensities and a shift to higher wavenumbers. The bands near 473 and 532 cm^{-1} for RS sample are assigned to the Si—O—Si and Al—O—Si, deformation vibrations, respectively. The small shift in the 532 cm^{-1} peak in the raw sample to 540 cm^{-1} in iron oxide coated sample confirms the involvement of the Si—O bond linkage in the modification. It is known that the IR spectrum of RS with absorption band at 667 cm^{-1} is due to bending Mg_3OH, and this band is directly related to the Mg content [35,36]. This band shifted to 677 cm^{-1} with less intensity, after oxide coating process. This change can be related to chemical composition of the octahedral layer.

Detailed analysis of IR spectra in the region between 1700 and 450 cm^{-1} can be used to discern the location of Pb(II) cations. The structural modifications of surface due to the adsorbed Pb(II) cations influenced the fundamental vibrations of OH and Si—O groups (Fig. 2a and b). The shift in the 782 cm^{-1} peak in the RS sample to 776 cm^{-1} in RS-Pb(II) sample confirms the involvement of the Si—O bond linkage in the Pb(II) adsorption process [37,38]. The change in the intensity of this band is also linked to Pb(II) adsorption, therefore this band can be considered as the indicator of Pb(II) adsorption process. After Pb(II) adsorption process, a decrease in wavenumber from 1643 to 677 cm^{-1} in the ICS sample to 1633 and 669 cm^{-1} was observed. The latter peaks also are less intense. This suggests that the lead adsorption may have been effected on the OH bending of water and the Mg_3OH bending vibration. Also, the peaks at 860 and 540 cm^{-1} disappeared, after lead adsorption onto ICS sample.

In the thermal analysis curves of clay minerals it is generally seen that the dehydration process occurs at low temperatures, the

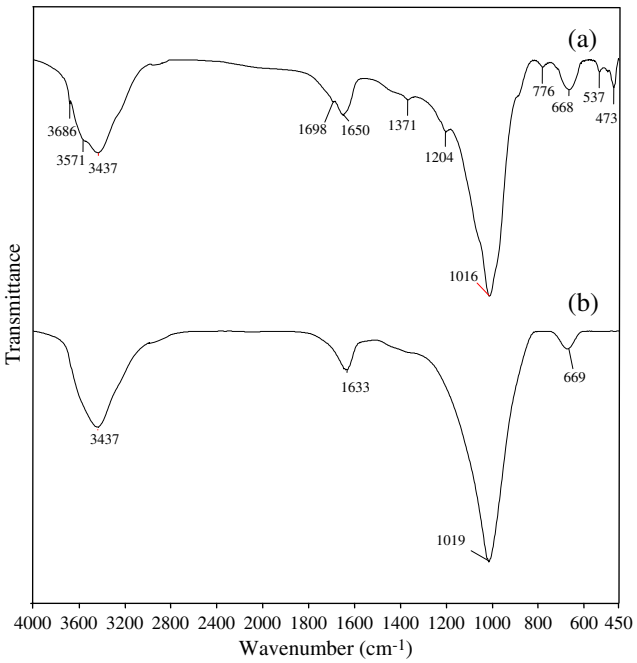

Fig. 2. IR spectra of the RS-Pb(II) (a) and ICS-Pb(II) (b) samples.

dehydroxylation occurs at intermediate temperatures and the phase transition takes place at relatively high temperatures. Furthermore, external clay components may also be exposed to thermal decomposition. The temperature values of dehydroxylation peaks shift to lower temperatures with the increase of the amount of metal cation in layers [39,40]. Thermal analysis (TG-DTA) profiles of the RS and ICS samples are shown in Fig. 3a and b and the related mass losses are given in Table 2. Thermal analysis data for ICS sample demonstrated mass losses by 3.6 and 3.6% in the temperature ranges 30–239 °C and 239–972 °C, respectively. These mass losses correspond to the decomposition of water and removal of structural OH of the clay, respectively. Thermal analysis data for RS exhibited mass losses by 6.7 at 30–376 °C and 6.6 at 376–987 °C due to the thermal evolution of moisture and interlayer water, and structural OH groups, respectively. The exothermal peak at 834 °C for RS and at 774 °C for ICS is assigned to the phase transformation of sepiolite to enstatite ($MgSiO_3$). The formation of enstatite necessitates Mg ions along the position of this cation. The formation of enstatite is controlled by the disposition of the cations within the octahedral sheet [41]. In ICS sample, the lower temperature for enstatite crystallization may be attributed to the lattice irregularities and dislocations within the crystals. Oliveira et al. [42] reported the reduction from Fe^{3+} to Fe^{2+} and from Fe^{2+} to Fe^0 in the temperature range of 550–750 °C for clay–iron oxides composites formed by precipitation of γ-Fe_2O_3 maghemite into the layers of the clays. In this case, iron oxides may participate in the formation of the spinel phase both in the trivalent and in the divalent state. Belver et al.

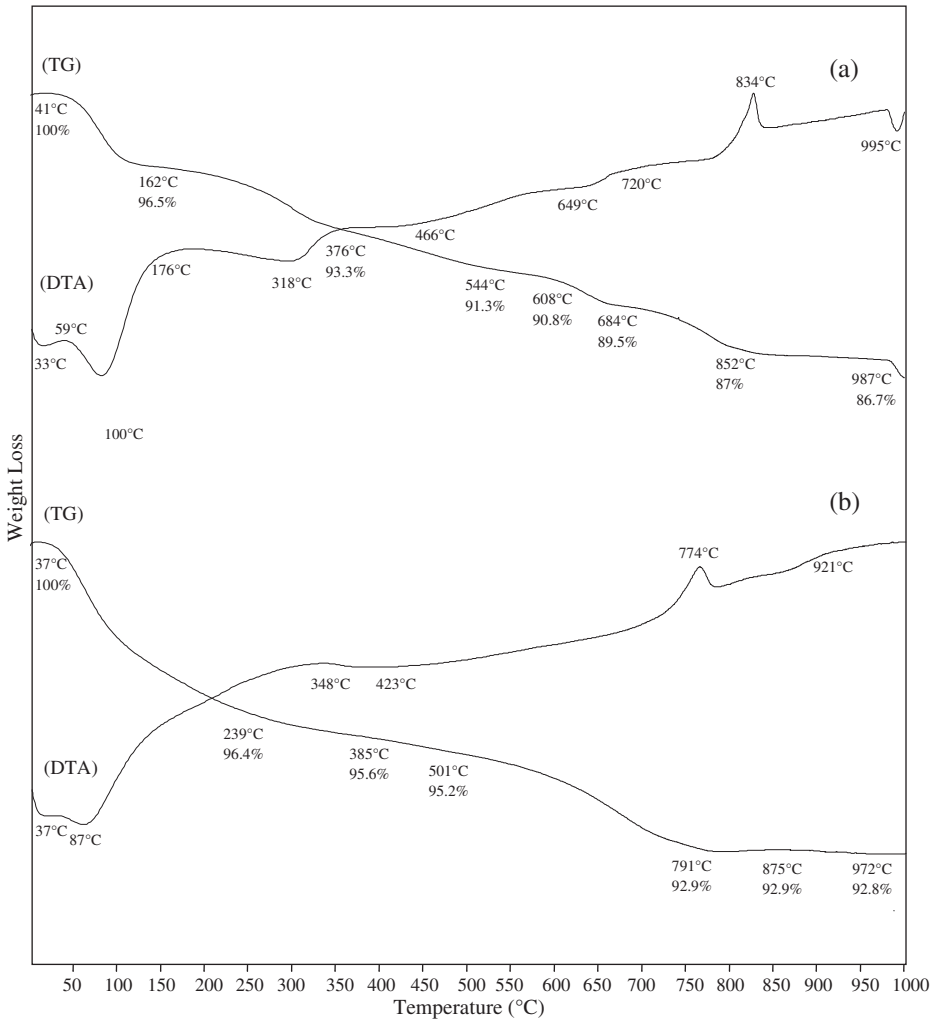

Fig. 3. Thermal analysis curves of RS (a) and ICS (b).

Table 2
Thermal analysis data of sepiolite samples.

Sample	Temperature range (°C)	Mass loss, Δm (%)	Total mass loss, Δm (%)
RS	41–162	3.5	13.3
	162–376	3.2	
	376–544	2.0	
	544–684	1.8	
	684–987	2.8	
ICS	37–239	3.6	7.2
	239–501	1.2	
	501–972	2.4	
RS-Pb(II)	42–165	3.9	12.8
	165–363	3.0	
	363–562	2.1	
	562–677	1.3	
	677–847	2.5	
ICS-Pb(II)	30–266	7.1	11.3
	266–740	2.8	
	740–952	1.4	

[43] reported that the reduction of the cations in octahedral holes resulted in a strong deleterious effect in the clay structure.

Comparison between thermal analyses of lead adsorbed sepiolite samples (Fig. 4a and b and Table 2) suggests that the ICS-Pb(II) sample contains higher external and zeolitic water than ICS and RS-Pb(II) samples. In the temperature range 30–400 °C, the weight losses are 6.7%, 4.6%, 6.9 and 7.8%, for RS, ICS, RS-Pb(II) and ICS-Pb(II) samples, respectively. These results show the differences in composition of octahedra and channels. It is concluded that crystal water bonded to octahedra at the edges of the channels can be linked by the different bond strengths both in RS-Pb(II) and ICS-Pb(II) samples.

3.2. Adsorption isotherms and parameters

The effect of temperature on the adsorption equilibrium was investigated under isothermal conditions in the temperature range of 298–318 K. The parameters for the isotherms obtained from Figs. 5–8 are presented in Table 3. The temperature of solution plays an important role in the whole adsorption process. The regression coefficients obtained from the Langmuir model and from the Freundlich model are higher than 0.94, suggesting that both the Langmuir and Freundlich models can be employed to describe the adsorption isotherms of RS and ICS for Pb(II) at the temperature range studied.

The Langmuir monolayer adsorption capacities varied from 51.36 to 78.51 mg/g for RS, these values varied from 75.79 to 119.34 mg/g for ICS in temperature range 298–318 K. The increase of adsorption capacities of RS and ICS for Pb(II) ions with increase in temperature indicates the endothermic nature of the adsorption processes. It is known that the adsorption process takes place by two consequent processes fast diffusion and slow complexation. The increase in temperature not only increases the rate of diffusion of the Pb(II) ions present in the bulk solution to the sepiolite surfaces but also increases the rate of complexation with the functional groups present on the sepiolite surfaces. The adsorption constant, K_L, also increased from 0.038 to 0.113 L/mg for RS and that for ICS increased from 0.023 to 0.048 L/mg with increasing temperature from 298 to 318 K. Large values of K_L indicates that the equilibrium is predominantly driven

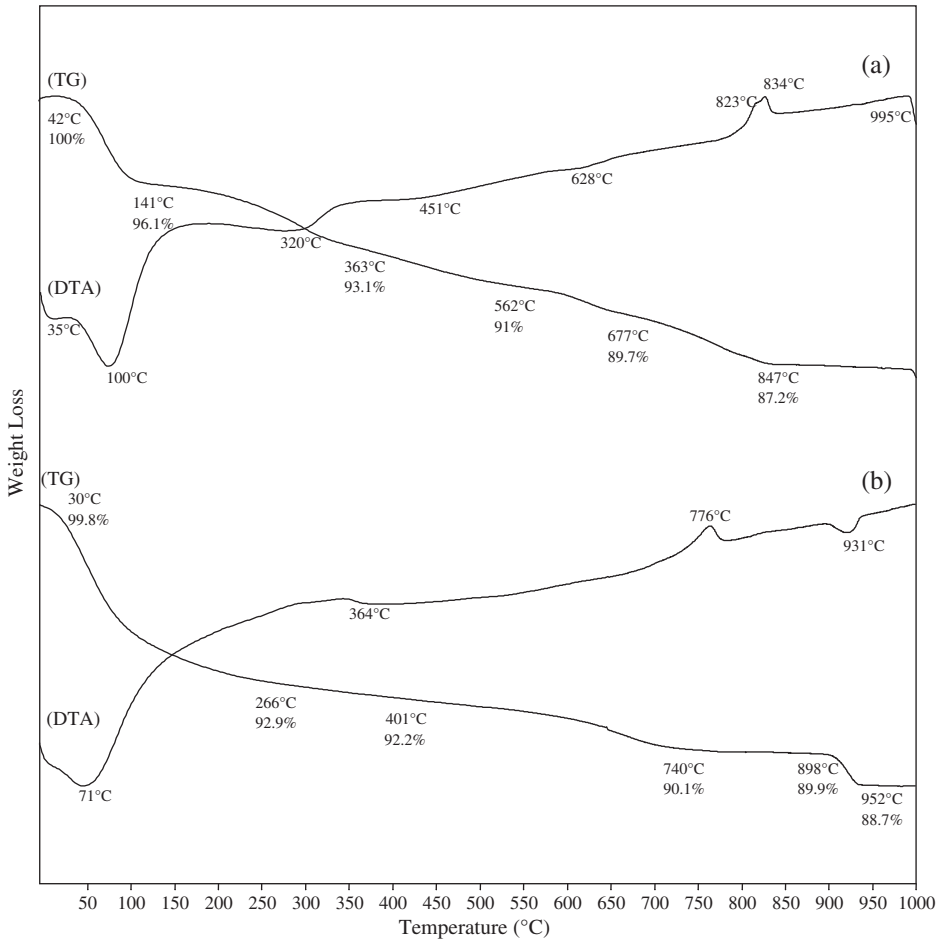

Fig. 4. Thermal analysis curves of RS-Pb(II) (a) and ICS-Pb(II) (b).

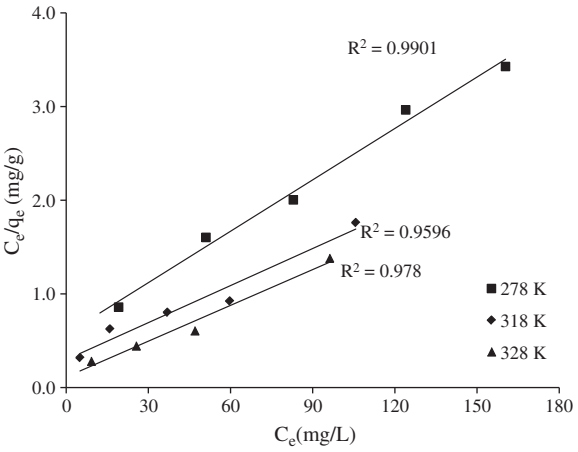

Fig. 5. Langmuir isotherm plot for the adsorption of Pb(II) onto RS sample at different temperatures. Squares, 298 K; diamonds, 318 K; triangles, 318 K, initial pH = 5.0, m = 1 g/L, ionic strength (IS) is 0.1 M $NaNO_3$ (controlled by $NaNO_3$).

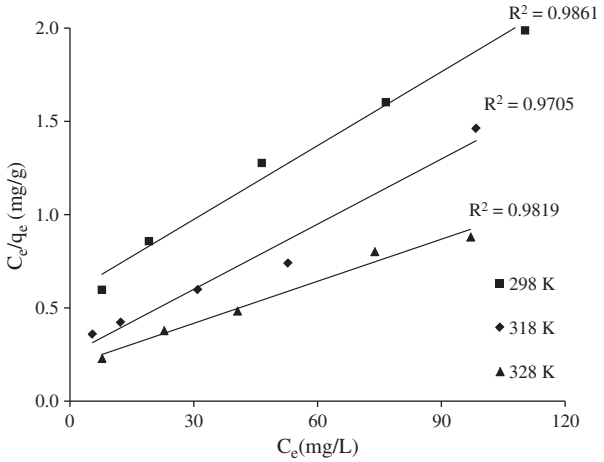

Fig. 7. Langmuir isotherm plot for the adsorption of Pb(II) onto ICS sample at different temperatures. Squares, 298 K; diamonds, 318 K; triangles, 318 K, initial pH = 5.0, m = 1 g/L, ionic strength (IS) is 0.1 M $NaNO_3$ (controlled by $NaNO_3$).

toward the right, leading to the formation of the adsorbate–adsorbent complex. The value of K_L for ICS is greater than that for RS. This result indicates that the adsorption of Pb(II) by ICS requests less energy than that of RS. Moreover, the high value of K_L has been related to specifically adsorbed metal at high energy surfaces with low dissociation constants; while the low value of K_L appears to be related to adsorption at low energy surfaces with high dissociation constants. So, the low K_L value of ICS may indicate that the adsorption of Pb(II) on ICS occurred mainly on specific adsorption positions.

The equilibrium data also fitted to Freundlich equation (Figs. 6 and 8), a fairly satisfactory empirical isotherm can be used for non-ideal adsorption. K_F relates the multilayer adsorption capacity and n intensity of adsorption, which varies with the heterogeneity of the adsorbent [44–46]. A relatively $n \ll 1$ indicates that adsorption intensity is favorable over the entire range of concentrations studied, while $n > 1$ means that adsorption intensity is favorable at high concentrations but much less at lower concentrations [46,47]. The Freundlich adsorption capacity (K_F) for the ICS sample was found to be lower than that for the RS. In the adsorption systems, the n values are higher than 1 which point out that adsorption intensity is favorable at high concentrations.

The works related to Pb(II) adsorption on raw sepiolite are scarce [48]. Bektaş et al. [40] have reported as 93.46–185.19 mg/g for Pb(II) ion adsorption at the temperature range 20–40 °C. The adsorption capacity of Pb(II) increased from 51.82 mg/g to 67.56 mg/g with the pH value of the lead solution increased from 4.0 to 6.0 at 295 K by Bektaş et al. [48]. The adsorption capacity of Pb(II) reduced from 93.46 mg/g to 56.18 mg/g with the particle size value of the sepiolite increased from 0.3–0.5 to 1.0–1.6 mm. The values of maximum adsorption capacities for RS and ICS samples calculated from the Langmuir isotherm in this study are compatible with reported values in the literature. The experimental data of the present investigation are comparable with the reported values by Bektaş et al. [48]. From this result, it also appears that the surface properties of RS could be improved upon modification of iron oxide.

3.3. Effect of ionic strength, pH and inorganic ligand

Adsorption of Pb(II) on sepiolite samples in the pH range of 2.0–5.5 is shown in Fig. 9 in 0.01, 0.05 and 0.1 M $NaNO_3$ solutions, respectively, The effect of ionic strength on metal adsorption process from aqueous solution is used to distinguish between ion exchange and surface complexation. The strong pH and ionic strength dependent adsorption indicates that adsorption of metal cation is controlled by ion exchange and surface complexation mechanism. Generally, surface complexation is pH dependent, whereas ion exchange is ionic strength dependent.

As shown in Fig. 9, the adsorption of Pb(II) onto RS is affected by ionic strength, especially at above pH 5.0. For example, when the concentration of $NaNO_3$ varied from 0.01 to 0.1 M, the adsorption of Pb(II) onto RS was decreased from 54.0 to 37.4 mg/g at pH 5.5. This

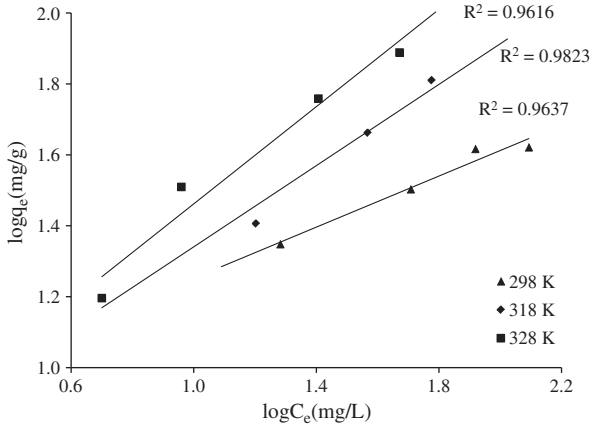

Fig. 6. Freundlich isotherm plot for the adsorption of Pb(II) onto RS sample at different temperatures. Squares, 298 K; diamonds, 318 K; triangles, 318 K, initial pH = 5.0, m = 1 g/L, ionic strength (IS) is 0.1 M $NaNO_3$ (controlled by $NaNO_3$).

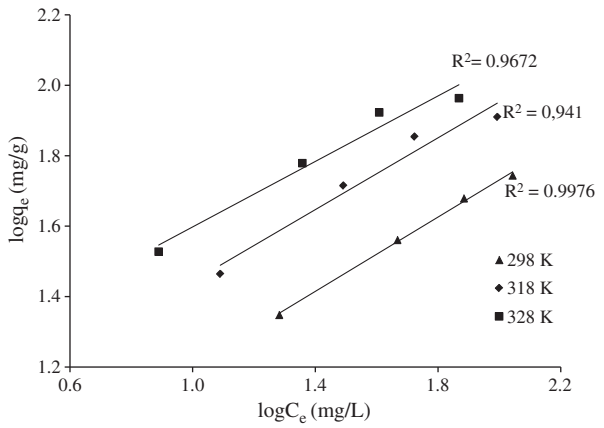

Fig. 8. Freundlich isotherm plot for the adsorption of Pb(II) onto ICS sample at different temperatures. Squares, 298 K; diamonds, 318 K; triangles, 318 K, initial pH = 5.0, m = 1 g/L, ionic strength (IS) is 0.1 M $NaNO_3$ (controlled by $NaNO_3$).

Table 3
Langmuir and Freundlich isotherm parameters for the adsorption of Pb(II) onto sepiolite samples.

Sample	T (K)	Langmuir constants			Freundlich constants		
		q_m (mg/g)	K_L (L/mg)	R^2	n	K_F ((mg/g)(L/mg)$^{1/n}$)	R^2
RS	298	51.36	0.038	0.990	2.78	7.80	0.961
	308	75.80	0.044	0.959	1.75	5.86	0.982
	318	78.51	0.113	0.978	1.46	5.98	0.963
ICS	298	75.79	0.023	0.986	1.90	4.75	0.967
	308	85.89	0.040	0.970	1.48	5.04	0.941
	318	119.34	0.048	0.981	1.37	9.44	0.997

may be due to the following two reasons: i — the effect of ionic strength on lead adsorption may be explained by the formation of outer-sphere complexes since Na^+ in the background electrolyte could compete with the lead ions adsorbed on the outer-sphere adsorption sites and reduce the adsorption, whereas Na^+ would not have competed for the inner-sphere sites [49]. ii — The electrostatic attraction seems to be a significant mechanism, as indicated by the results where at high ionic strength, the increased amount of $NaNO_3$ can help to render the surface of the ICS not easily accessible to Pb(II) ions. According to the electrical diffuse double layer theory, when solid adsorbent is in contact with sorbate species in solution, they are bound to be surrounded by an electrical diffused double layer, the thickness of which is significantly expanded by the presence of electrolyte. Such expansion may be inhibited by the approach between ICS particles and Pb(II) cations. Due to these reasons, the decreasing amount of adsorbed lead ions with increasing $NaNO_3$ concentration may be explained by the ions at the sepiolite surface contributing to the adsorption and complexation of Pb(II). The ionic strength dependent adsorption indicates that ion exchange or outer-sphere complexation contributes to Pb(II) adsorption on RS at a pH value above 5.5. From Fig. 9, it can be seen that the adsorption of Pb(II) on ICS is weakly dependent on the ionic strength of the medium. The ionic strength independent adsorption at the pH value above 5.5 suggests that inner-sphere complexation/chemical adsorption is the main adsorption mechanism of Pb(II) onto ICS.

Fig. 10 shows the adsorption curve of Pb(II) on sepiolite samples as a function of pH in 0.01 M $NaNO_3$ and NaCl solutions, respectively. The adsorbed Pb(II) in the presence of inorganic ligands may be also attributed to a high specificity of the surfaces for Pb(II) relative to ligands. The adsorption of Pb(II) ions by the ICS sample was influenced by the presence of Cl^- and NO_3^- (Fig. 10). The amount of

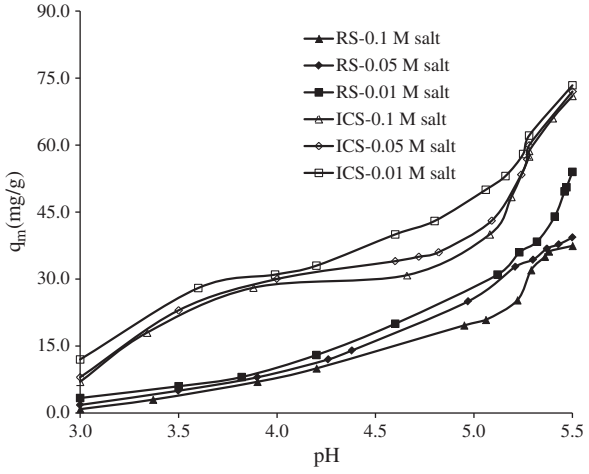

Fig. 9. Adsorption of Pb(II) (124.7 mg/L) by RS and ICS (1 g/L) samples as function of pH and ionic strength. Squares, 0.1 M; diamonds 0.05 M; triangles, 0.01 M.

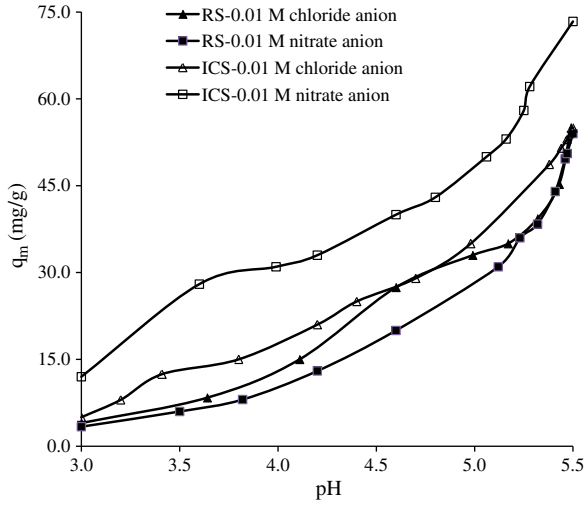

Fig. 10. Adsorption of Pb(II) (124.7 mg/L) by RS and ICS (1 g/L) samples as function of pH and in the presence of inorganic ligands. Squares, 0.01 M NO_3^-; triangles, 0.01 M Cl^-.

adsorbed lead on ICS sample in the 0.01 M Cl^- and NO_3^- systems at pH 5.5 are 55.0 and 73.3%, respectively. The results demonstrate that anions affect Pb(II) adsorption on ICS sample. This phenomenon may be contributed to the facts that: (I) Cl^- and NO_3^- can form soluble complexes with Pb(II) ion in solution (e.g. $PbCl_x^{(2-x)-}$, $Pb(NO_3)_x^{(2-x)-}$) and by that reduce or completely disable sorption at sepiolite. (II) NO_3^- ligand form less stable complex with Pb(II), which result with higher effect at sorption efficacy. (III) Adsorption of Cl^- to sepiolite surface is a little easier than NO_3^- and Cl^- adsorption on the surface of ICS that changes the surface properties of ICS and decreases the availability of binding sites for Pb(II). This result suggests that the adsorption of Cl^- to ICS surface is easier than NO_3^-, and Cl^- adsorption on the surface of ICS changes the surface properties of ICS and decreases the availability of binding sites for Pb(II).

3.4. Thermodynamic studies

ΔG, ΔH and ΔS values were calculated as −15.46 kJ/mol (at 298 K), 47.78 kJ/mol and 212 J/mol K for RS sample, and −16.03 kJ/mol (at 298 K), 47.78 kJ/mol and 213 J/mol K for ICS sample (Table 4).

The negative values for the Gibbs free energy change, ΔG, show that the adsorption process for the two sepiolite samples is spontaneous and the degree of spontaneity of the reaction increases with increasing temperature. The increase in adsorption with temperature may be attributed to the increase in the number of active surface sites available for adsorption on the adsorbent and the decrease in the thickness of the boundary layer surrounding the adsorbent with temperature. The values of ΔG are negative for the ICS suggesting that the adsorption process for this material is spontaneous. The positive values of ΔH indicate the endothermic behavior of adsorption reaction. This fact was proved by the increase in the adsorption of Pb(II) with temperature in Section 3.2. The positive values of ΔH suggest that a large amount of heat is consumed to transfer the Pb(II) ions from aqueous into the solid phase. This result

Table 4
Thermodynamic parameters for the adsorption of Pb(II) (124.7 mg/L) onto sepiolite samples.

Sample	ΔH (kJ/mol)	ΔS (J/mol K)	ΔG (kJ/mol)			R^2
			298	308	318	
RS	47.78	212	−15.46	−17.58	−19.70	0.975
ICS	47.48	213	−16.03	−18.16	−20.30	0.977

may be explained by the following reasons: the higher Pb(II) removal due to increasing temperature may be attributed to the interaction taking place between the adsorption sites of ICS and Pb(II). The exchange of the Pb(II) with H^+ needs the bond breaking of OH groups on ICS surface, which is an endothermic process. Also, the sorption of Pb(II) requires a diffusion process, which is an endothermic process; i.e., the rise of temperature favors Pb(II) transport within the particles of ICS. The positive values of ΔS reflect the affinity of the sepiolite samples for Pb(II) and indicate the increased randomness at the solid–solution interface due to the decreases in the hydration of the adsorbing Pb(II) cations. Pb(II) cations must give up a larger share of their hydration water before they could introduce the surface. Such a release of water from Pb(II) cations causes the positive values of ΔS.

The experimental adsorption thermodynamic data of the present investigation are comparable with reported values. Bektaş et al. [48] have reported that ΔG°, ΔH° and ΔS° for adsorption of Pb(II) on sepiolite have values of −0.205 kJ/mol, 6.606 kJ/mol, and 0.205 kJ/mol K, respectively. Huang [50] evaluated that ΔG°, ΔH° and ΔS° of Pb(II) adsorption on Al_2O_3-supported iron oxide were −19.4 kJ mol^{-1} (at 318 K), 25.73 kJ mol^{-1} and 0.113 J $mmol^{-1}$ K^{-1}, respectively. Eren [51] has found that ΔG°, ΔH° and ΔS° for Pb(II) adsorption on iron-oxide coated bentonite are −21.74 kJ mol^{-1} (at 303 K), 69 kJ mol^{-1} and 299 J mol^{-1} K^{-1}, respectively. Manju et al. [52] have reported that ΔH° and ΔS° for adsorption of Pb(II) on polyacrylamide-grafted iron(III) oxide are 42.66 kJ/mol and 162.11 J/K mol, respectively.

3.5. Desorption of Pb(II)

The result of the desorption test carried on sepiolite samples using different HNO_3 concentrations is presented in Fig. 11. As seen, the desorption efficiency increased with the increase in HNO_3 concentration. No significant desorption was observed in the deionized water; while almost 42 and 34% desorption for RS and ICS sepiolite samples, respectively, was obtained at 0.1 M HNO_3. This suggests that the adsorption of Pb(II) onto sepiolite samples is irreversible, and the bonding between the active sites and the adsorbed Pb(II) is strong. The result of the desorption test carried on RS and ICS samples using 0.1 M HNO_3 solution is presented in Table 5. After three cycles, the adsorption capacity of the RS and ICS decreased from 34% to 20% and from 42% to 35%, respectively. The desorption of Pb(II) by 0.1 M HNO_3 decreases from 24% in the first cycle to 2% in the third cycle for RS while that of ICS decreased from 26% in the first cycle to 5% in the third cycle. The lower cation exchange capacity of the sepiolite samples can be considered to be responsible for the lower desorption percentage for Pb(II). This indicated that more Pb(II) ions are adsorbed on specific sites than on the nonspecific sites.

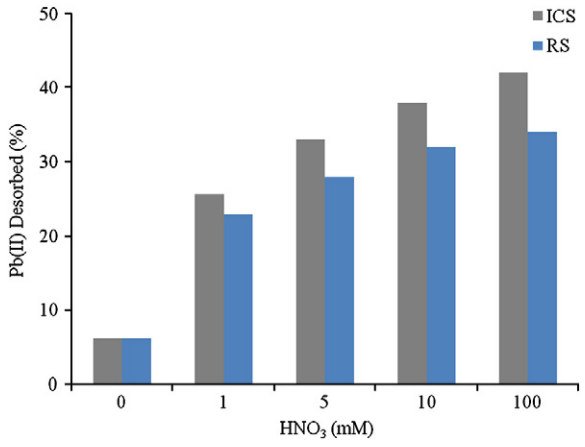

Fig. 11. Desorption of Pb(II) from Pb(II)-loaded sepiolite samples using a different concentration of HNO_3 solution. Pb(II) = 62 mg/L, adsorbent amount: 1 g/L, contact time: 2 h, T = 298 K.

Table 5
Three cycles of Pb(II) adsorption–desorption using 0.1 M HNO_3 as desorbing agent. Pb(II) = 62 mg/L, adsorbent amount: 1 g/L, contact time: 2 h, T = 298 K.

Sample	No of cycles	Adsorption	Desorption
RS	1	34	24
	2	26	3
	3	20	2
ICS	1	42	24
	2	36	6
	3	35	5

4. Conclusions

In the present work, a cheap, readily available and effective adsorbent material has identified sepiolite as a potentially attractive adsorbent for the treatment of Pb(II) contaminated aqueous solutions after modification with iron oxide. The adsorption of Pb(II) by sepiolite samples was influenced by pH, ionic strength, and the presence of Cl^-. The adsorption isotherm studies indicate that the adsorption of Pb(II) follows both the Langmuir and Freundlich isotherms. From the values of the Langmuir monolayer capacity, q_m, it is concluded that the treatment with iron oxide does increase the number of adsorption sites to a large extent. Observed perturbation on the zeolitic and bound water vibrations of sepiolite indicates that some of iron oxide particles enter the interior channels and replace zeolitic water molecules. Thermal analysis results point out to differences in bond strengths between octahedral cations and H_2O, differences which can be produced by both octahedra and channels populations. Since there is a huge deposit of sepiolite in Turkey, there is great potential for its utilization in wastewater treatment.

References

[1] C.-I. Lee, W.-F. Yang, C.-I. Hsieh, Removal of copper (II) by manganese-coated sand in a liquid fluidized-bed reactor, J. Hazard. Mater. 114 (2004) 45–51.
[2] Y. Li, X. Wang, S. Guo, D. Dong, Cu and Zn adsorption onto non-residual and residual components in the natural surface coatings samples (NSCSs) in the Songhua River, China, Environ. Pollut. 143 (2006) 221–227.
[3] S.R. Huelin, H.P. Longerich, D.H.C. Wilton, B.J. Fryer, Y. Li, X. Wang, S. Guo, D. Dong, The determination of trace elements in Fe–Mn oxide coatings on pebbles using LA-ICP-MS, J. Geochem. Explor. 91 (2006) 110–124.
[4] B. Rusch, K. Hanna, B. Humbert, Characterization and surface reactivity of iron coating phases, Colloid Surf. A 353 (2010) 172–180.
[5] Y. Xu, L. Axe, Synthesis and characterization of iron oxide-coated silica and its effect on metal adsorption, J. Colloid Interf. Sci. 282 (2005) 11–19.
[6] R.L. Vaughan Jr., B.E. Reed, Modeling As(V) removal by a iron oxide impregnated activated carbon using the surface complexation approach, Water Res. 39 (2005) 1005–1014.
[7] W. Chen, R. Parette, J. Zou, F.S. Cannon, B.A. Dempsey, Arsenic removal by iron-modified activated carbon, Water Res. 41 (2007) 1851–1858.
[8] M. Nachtegaal, D.L. Spark, Clay effect of iron oxide coatings on zinc sorption mechanisms at the clay-mineral/water interface, J. Colloid Interf. Sci. 276 (2004) 13–23.
[9] S. Lazarevic, I. Jankovic-Castvan, D. Jovanovic, S. Milonjic, D. Janackovic, R. Petrovic, Adsorption of Pb^{2+}, Cd^{2+} and Sr^{2+} ions onto natural and acid-activated sepiolites, Appl. Clay Sci. 37 (2007) 47–57.
[10] M. Alkan, G. Tekin, H. Namli, FTIR and zeta potential measurements of sepiolite treated with some organosilanes, Micropor. Mesopor. Mat. 84 (2005) 75–83.
[11] A. Corma, H. Garcia, A. Leyva, A. Primo, Alkali-exchanged sepiolites containing palladium as bifunctional (basic sites and noble metal) catalysts for the Heck and Suzuki reactions, Appl. Catal. A Gen. 257 (2004) 77–83.
[12] L.I. Vico, Acid–base behaviour and Cu^{2+} and Zn^{2+} complexation properties of the sepiolite/water interface, Chem. Geol. 198 (2003) 213–222.
[13] K. Kaneda, T. Kiriyama, T. Hiraoka, T. Imanaka, Preparation of divalent Pd(II) species on sepiolite and its catalysis of olefin dimerizations, J. Mol. Catal. 48 (1988) 343–347.
[14] J.A. Anderson, L. Daza, S. Damyanova, J.L.G. Fierro, M.T. Rodrigo, Hydrogenation of styrene over nickel/sepiolite catalysts, Appl. Catal. A Gen. 113 (1994) 75–88.
[15] F.M. Bautista, D. Luna, J. Luque, J.M. Marinas, J.F. Sánchez-Royo, Gas-phase selective oxidation of chloro- and methoxy-substituted toluenes on TiO_2–sepiolite supported vanadium oxides, Appl. Catal. A Gen. 352 (2009) 251–258.
[16] J. Ma, E. Bilotti, T. Peijs, J.A. Darr, Preparation of polypropylene/sepiolite nanocomposites using supercritical CO_2 assisted mixing, Eur. Polym. J. 43 (2007) 4931–4939.
[17] S. Xie, S. Zhang, F. Wang, M. Yang, R. Séguéla, J.-M. Lefebvre, Preparation, structure and thermomechanical properties of nylon-6 nanocomposites with lamella-type and fiber-type sepiolite, Compos. Sci. Technol. 67 (2007) 2334–2341.

[18] S. Xie, S. Zhang, F. Wang, M. Yang, R. Séguéla, J.M. Lefebvre, E. Franchini, J. Galy, J.F. Gérard, Sepiolite-based epoxy nanocomposites: relation between processing, rheology, and morphology, J. Colloid. Interf. Sci. 329 (2009) 38–47.
[19] Q.K. Wang, T. Matsuura, C.Y. Feng, M.R. Weir, C. Detellier, E. Rutadinka, R.L. Van Mao, The sepiolite membrane for ultrafiltration, J. Membr. Sci. 184 (2001) 153–163.
[20] M.R. Weir, E. Rutinduka, C. Detellier, C.Y. Feng, Q. Wang, T. Matsuura, R. Le Van Mao, Fabrication, characterization and preliminary testing of all-inorganic ultrafiltration membranes composed entirely of a naturally occurring sepiolite clay mineral, J. Membr. Sci. 182 (2001) 41–50.
[21] M. Doğan, Y. Özdemir, M. Alkan, Adsorption kinetics and mechanism of cationic methyl violet and methylene blue dyes onto sepiolite, Dyes Pigm. 75 (2007) 701–713.
[22] M. Alkan, Ö. Demirbaş, S. Çelikçapa, M. Doğan, Sorption of acid red 57 from aqueous solution onto sepiolite, J. Hazard. Mater. 116 (2004) 135–145.
[23] M. Doğan, Y. Turhan, M. Alkan, H. Namli, P. Turan, Ö. Demirbaş, Functionalized sepiolite for heavy metal ions adsorption, Desalination 230 (2008) 248–268.
[24] M.F. Brigatti, C. Lugli, L. Poppi, Kinetics of heavy-metal removal and recovery in sepiolite, Appl. Clay Sci. 16 (2000) 45–57.
[25] F.C.M.J.M. Van Delft, A.J. Den Hartog, D.J.W. Ijdo, V. Ponec, G.H. Vurrens, A.M. Van Der Kraan, Oxidation and dehydrogenation of alcohols by glauconite, a natural Fe (II)- and Fe(III)-containing sheet silicate, and ferri-sepiolite, its molecular sieve analogue, J. Mol. Catal. 60 (1990) 109–125.
[26] M.L. Occelli, J.T. Hsu, L.G. Galaya, Propylene oligomerization over molecular sieves: part I. Zeolite effects on reactivity and liquid product selectivities, J. Mol. Catal. 32 (1985) 377–390.
[27] G.A.M. Darder, P. Aranda, E. Ruiz-Hitzky, Multifunctional materials based on graphene-like/sepiolite nanocomposites, Appl. Clay Sci. 47 (2010) 203–211.
[28] G. Sandi, K.A. Carrado, R.E. Winans, C.S. Johnson, R. Csencsits, Carbons for lithium battery applications prepared using sepiolite as an inorganic template, J. Electrochem. Soc. 146 (1999) 3644–3648.
[29] G. Sandí, R.E. Winans, S. Seifert, K.A. Carrado, In situ SAXS studies of the structural changes of sepiolite clay and sepiolite–carbon composites with temperature, Chem. Mater. 14 (2002) 739–742.
[30] E. Eren, H. Gumus, N. Ozbay, Equilibrium and thermodynamic studies of Cu(II) removal by iron oxide modified sepiolite, Desalination 262 (2010) 43–49.
[31] I. Langmuir, The adsorption of gases on plane surfaces of glass, mica and platinum, J. Am. Soc. 40 (1918) 1361–1403.
[32] H. Freundlich, Uber die adsorption in losungen, Z. Phys. Chem. (Leipzig) 57 (1906) 385–470.
[33] E. Eren, Removal of copper ions by modified Unye clay, Turkey, J. Hazard. Mater. 159 (2008) 235–244.
[34] R.L. Frost, Y. Xi, H. He, Synthesis, characterization of palygorskite supported zero-valent iron and its application for methylene blue adsorption, J. Colloid Interf. Sci. 341 (2010) 153–161.
[35] A. Chahi, S. Petit, A. Decarreau, Infrared evidence of dioctahedral–trioctahedral site occupancy in palygorskite, Clay Clay Miner. 50 (2002) 306–313.
[36] M. Suárez, E. García-Romero, FTIR spectroscopic study of palygorskite: influence of the composition of the octahedral sheet, Appl. Clay Sci. 31 (2006) 154–163.
[37] D.A. Mckeown, J.E. Post, E.S. Etz, Vibrational analysis of palygorskite and sepiolite, Clay Clay Miner. 50 (2002) 667–680.
[38] R.L. Frost, O.B. Locos, H. Ruan, J.T. Kloprogge, Near-infrared and mid-infrared spectroscopic study of sepiolites and palygorskites, Vib. Spectrosc. 27 (2001) 1–13.
[39] M.S. Hassan, N.A. Abdel-Khalek, Beneficiation and applications of an Egyptian bentonite, Appl. Clay Sci. 13 (1998) 99–115.
[40] E. Eren, B. Afsin, An investigation of Cu(II) adsorption by raw and acid-activated bentonite: a combined potentiometric, thermodynamic, XRD, IR, DTA study, J. Hazard. Mater. 151 (2008) 682–691.
[41] G. Kulbicki, High temperature phases in sepiolite, attapulgite and saponite, Am. Miner. 44 (1959) 752–764.
[42] L.C.A. Oliveira, R.V.R.A. Rios, J.D. Fabris, K. Sapag, V.K. Garg, R.M. Lago, Clay–iron oxide magnetic composites for the adsorption of contaminants in water, Appl. Clay Sci. 22 (2003) 169–177.
[43] C. Belver, M.A. Bañares-Muñoz, M.A. Vicente, Fe-saponite pillared and impregnated catalysts: I. Preparation and characterisation, Appl. Catal. B Environ. 50 (2004) 101–112.
[44] P. Balaz, A. Alacova, J. Briancin, Sensitivity of Freundlich equation constant 1/n for zinc sorption on changes induced in calcite by mechanical activation, Chem. Eng. J. 114 (2005) 115–121.
[45] Y.E. Mouzdahir, A. Elmchaouri, R. Mahboub, A. ElAnssari, A. Gil, S.A. Korili, M.A. Vicente, Interaction of stevensite with Cd^{2+} and Pb^{2+} in aqueous dispersions, Appl. Clay Sci. 35 (2007) 47–58.
[46] Y.S. Al-Degs, M.I. El-Barghouthi, A.A. Issa, M.A. Khraisheh, G.M. Walker, Sorption of Zn(II), Pb(II), and Co(II) using natural sorbents: equilibrium and kinetic studies, Water Res. 40 (2006) 2645–2658.
[47] B.H. Hameed, A.L. Ahmad, K.N.A. Latif, Adsorption of basic dye (methylene blue) onto activated carbon prepared from rattan sawdust, Dyes Pigm. 75 (2007) 143–149.
[48] N. Bektaş, B.A. Ağım, S. Kara, Kinetic and equilibrium studies in removing lead ions from aqueous solutions by natural sepiolite, J. Hazard. Mater. 112 (2004) 115–122.
[49] X. Guo, S. Zhang, X.-Q. Shan, Adsorption of metal ions on lignin, J. Hazard. Mater. 151 (2008) 134–142.
[50] Y.H. Huang, C.L. Hsueh, C.P. Huang, L.C. Su, C.Y. Chen, Adsorption thermodynamic and kinetic studies of Pb(II) removal from water onto a versatile Al_2O_3-supported iron oxide, Sep. Purif. Technol. 55 (2007) 23–29.
[51] E. Eren, Removal of lead ions by Unye (Turkey) bentonite in iron and magnesium oxide-coated forms, J. Hazard. Mater. 165 (2009) 63–70.
[52] G.N. Manju, K. Anoop Krishnan, V.P. Vinod, T.S. Anirudhan, An investigation into the sorption of heavy metals from wastewaters by polyacrylamide-grafted iron (III) oxide, J. Hazard. Mater. 91 (2002) 221–238.